

BBN constraints on dark radiation isocurvature

Peter Adshead, Gilbert Holder, and Pranjal Ralegankar

Department of Physics, University of Illinois at Urbana-Champaign, Urbana, IL 61801, USA

E-mail: adshead@illinois.edu, gholder@illinois.edu, pranjal6@illinois.edu

Abstract. The existence of dark radiation that is completely decoupled from the standard model in the early Universe leaves open the possibility of an associated dark radiation isocurvature mode. We show that the presence of dark radiation isocurvature leads to spatial variation in the primordial abundances of helium and deuterium due to spatial variation in N_{eff} during Big Bang nucleosynthesis. We use the result to constrain the existence of such an isocurvature mode on scales down to ~ 1 Mpc scales. By measuring the excess variance in the primordial helium to hydrogen and deuterium to hydrogen ratio in different galaxies, we constrain the variance in average isocurvature in a galaxy to be less than $0.13/\Delta\bar{N}_{\text{eff}}$ at 95% confidence. Here $\Delta\bar{N}_{\text{eff}}$ is the spatially averaged increase in N_{eff} due to the additional dark radiation component.

Contents

1	Introduction	1
2	Inhomogenous Big Bang Nucleosynthesis through dark radiation isocurvature	2
3	Constraints from He/H and D/H data	4
4	Discussion and conclusions	7
A	Dark radiation isocurvature as spatially varying N_{eff}	9

1 Introduction

Upcoming stage 4 cosmic microwave background (CMB) experiments will make exquisite measurements of the energy content of the Universe [1]. These measurements will improve the constraint on the contribution of free-streaming radiation (through the effective number of relativistic species N_{eff}) by an order of magnitude over current constraints. A measurement of N_{eff} consistent with the standard model (SM) prediction of $N_{\text{eff}} = 3.044$ [2–5] will place extremely strong constraints on particle content beyond the SM [6].

Alternatively, these measurement could reveal the existence of additional light-particles (dark radiation) beyond the SM by measuring $N_{\text{eff}} \neq 3.044$ at high significance. If these additional particles were ever in thermal equilibrium with the standard model, they will exhibit the usual adiabatic fluctuations in their density (see, e.g. [7]), and their effects on cosmology would be indistinguishable from additional neutrinos. However, this dark radiation may be completely decoupled from the standard model sector. In this decoupled scenario, fluctuations in the dark radiation density may be independent of the density fluctuations in the visible sector—there may be a dark-radiation isocurvature mode. Isocurvature modes are generically predicted by cosmological theories that have a second clock beyond the SM temperature field [8]. In this work we remain agnostic to the exact origin of such an initial condition and leave detailed model-building to future work.

The presence of dark radiation isocurvature affects the cosmic microwave background (CMB). Earlier work [9] constrained neutrino + dark radiation isocurvature to be less than $\sim 10^{-5}$ at scales around 500 Mpc using data from WMAP and ACT (see also Ref. [10] for non-Gaussian dark radiation isocurvature constraints). Planck is sensitive to dark-radiation isocurvature for scales ≥ 10 Mpc [11]. However, the inability to observe CMB fluctuations on angular sizes smaller than ~ 5 arcmins prohibits the estimation of isocurvature constraints on smaller scales [12]. In this work we probe dark radiation isocurvature down to ~ 1 Mpc scales through its impact on Big Bang nucleosynthesis (BBN).

BBN is a period in the early universe when the SM plasma became cold enough for the free protons and neutrons to combine and form the first nuclei. This process primarily produces Helium and Deuterium (along with trace amounts of tritium and Lithium). Adiabatic fluctuations during BBN do not lead to spatial variations in the outcome of BBN. This result follows directly from the separate universe picture—different patches of the Universe with differing density fluctuations simply appear to be a little older or younger as viewed by

local observers. Since the local physics is identical, the outcome is identical. The presence of isocurvature during BBN can change the story by changing the physical conditions locally in a way that is distinguishable from a local shift in the clock. In this way, isocurvature leads to spatial variation in primordial elemental yields. Spatial variations in the yields of He/H and D/H during BBN would then lead to corresponding differences in abundances in widely separated locations. To date, baryon isocurvature modes as a source of inhomogeneous BBN have been extensively studied in the literature [13–16]. In this work we consider the effect of dark radiation isocurvature on the primordial elemental abundances from BBN.

Our results can be summarized as follows. We demonstrate that the presence of dark-radiation isocurvature leads to spatially varying elemental abundances. As a result, galactic He/H and D/H ratios are sensitive to dark-radiation isocurvature on galactic scales, ~ 1 Mpc. We use data on Helium abundances in nearby galaxies [17] and Deuterium abundances in high-redshift Lyman- α absorption systems [18] to place constraints on the existence of dark radiation isocurvature. We constrain the variance of average isocurvature fluctuations in galaxies, to be less than $0.13/\Delta\bar{N}_{\text{eff}}$ at 2σ confidence for scales around ~ 1 Mpc. Here $\Delta\bar{N}_{\text{eff}}$ is the spatially averaged increase in N_{eff} due to the additional dark radiation component. In the absence of any dark-radiation, i.e. $\Delta\bar{N}_{\text{eff}} = 0$, our constraints are relaxed as expected.

This paper is organized as follows. In section 2, we show how dark-radiation isocurvature leads to spatially varying BBN yields and demonstrate that this leads to differences in the primordial abundances of light elements in different galaxies. In section 3, we use excess variance in existing He/H and D/H data to place constraints on dark-radiation isocurvature. We conclude in section 4. Finally, in appendix A we use the separate universe approach to demonstrate how dark-radiation isocurvature leads to spatially varying ΔN_{eff} .

2 Inhomogeneous Big Bang Nucleosynthesis through dark radiation isocurvature

In this section we demonstrate the impact of dark-radiation isocurvature on BBN. We first show how the effect of dark-radiation isocurvature on BBN is distinct from the more studied baryon-isocurvature case [13–16]. We then demonstrate that dark-radiation isocurvature leads to spatially varying N_{eff} that in turn causes spatial variation in primordial abundances of hydrogen and helium.

The elemental abundances produced by BBN are primarily determined by two processes: the weak processes which convert neutrons to protons, and by the deuterium formation process that forms deuterium from all the remaining neutrons. The temperature at which deuterium formation begins, T_{nuc} , is insensitive to the Hubble rate and is primarily determined by the baryon-to-photon ratio. Baryon-isocurvature modes cause the baryon-to-photon ratio to vary spatially. This in turn leads to a spatially varying T_{nuc} , and to spatial variations of the resulting elemental abundances. In contrast, a dark-radiation isocurvature mode leads to a spatially varying N_{eff} , as we show below. The abundance of neutrons at T_{nuc} is sensitive to the Hubble rate at T_{nuc} , and since N_{eff} affects the Hubble rate through the Friedmann equation, an inhomogeneous N_{eff} leads to an inhomogeneous abundance of neutrons at T_{nuc} .

To show how dark-radiation isocurvature leads to spatial variation in N_{eff} , we first highlight the relation between dark-radiation energy density and N_{eff} . At $T \sim 1$ MeV, before BBN begins, neutrinos have chemically decoupled from SM plasma and thus evolve adiabatically like dark radiation. We can therefore absorb the density of dark radiation, ρ_{DR} , into an extra neutrino component [19],

$$\Delta N_{\text{eff}} = \left[\frac{8}{7} \left(\frac{11}{4} \right)^{4/3} \frac{\rho_{DR}}{\rho_\gamma} \right]_{\text{today}}. \quad (2.1)$$

Thus ΔN_{eff} depends on the ratio of homogeneous densities of dark-radiation to SM.

In appendix A, using the separate universe principle [20, 21], we show that long wavelength dark radiation isocurvature, S_{DR} , can be absorbed into the homogeneous densities for super-horizon sized patches. Isocurvature between the dark-radiation and the photon bath is defined as

$$S_{DR} = \frac{3}{4} \left(\frac{\delta \rho_{DR}}{\rho_{DR}} - \frac{\delta \rho_\gamma}{\rho_\gamma} \right). \quad (2.2)$$

Since the photon fluctuations are assumed to be adiabatic together with the SM density fluctuations, isocurvature between the dark-radiation and the photon bath is equivalent to isocurvature between the dark-radiation and the SM plasma. A super-horizon patch characterized by some window function, $W_{\lambda/2}$, that has support within a sphere of radius $\lambda/2$, has an average isocurvature, ΔS_{DR} , given by

$$\Delta S_{DR} = \frac{\int_0^\infty d^3x S_{DR}(\vec{x}) W_{\lambda/2}(\vec{x})}{\int d^3x W_{\lambda/2}(\vec{x})}. \quad (2.3)$$

The dark-radiation isocurvature causes each such patch to observe ΔN_{eff} given by (see appendix A.3)

$$\Delta N_{\text{eff}} = \Delta \bar{N}_{\text{eff}} \left(\frac{1 + \frac{4}{3} \frac{1}{1 + \rho_{DR}/\rho_{SM}} \Delta S_{DR}}{1 - \frac{4}{3} \frac{\rho_{DR}/\rho_{SM}}{1 + \rho_{DR}/\rho_{SM}} \Delta S_{DR}} \right) \approx \Delta \bar{N}_{\text{eff}} \left(1 + \frac{4}{3} \Delta S_{DR} \right), \quad (2.4)$$

where the over-bar denotes a spatial average, and ρ_{SM} is the density of SM plasma. In the second equality we have assumed that $\rho_{DR} \Delta S_{DR} / \rho_{SM} \ll 1$, or equivalently $\Delta \bar{N}_{\text{eff}} \Delta S_{DR} \ll 1$. Because ΔS_{DR} takes different values in different regions, dark-radiation isocurvature leads to spatial variations in ΔN_{eff} .

In the presence of a dark-radiation isocurvature mode, regions of the Universe that were causally disconnected during BBN have different primordial abundances of light elements due to their different values of ΔN_{eff} . For example, the D/H ratio, D , is primarily a function of ΔN_{eff} and the baryon fraction $\Omega_b h^2$. Assuming small fluctuations in ΔN_{eff} , the fluctuation in D is given by

$$D \approx \bar{D} + \left. \frac{\partial D}{\partial \Delta N_{\text{eff}}} \right|_{\Delta \bar{N}_{\text{eff}}} (\Delta N_{\text{eff}} - \Delta \bar{N}_{\text{eff}}), \quad (2.5)$$

where $\bar{D} = D(\Delta \bar{N}_{\text{eff}}, \Omega_b h^2)$. This gives us a direct relation between the variance in D , given by σ_d , and the variance in ΔN_{eff} fluctuations

$$\sigma_d = \left. \frac{\partial D}{\partial \Delta N_{\text{eff}}} \right|_{\Delta \bar{N}_{\text{eff}}} \sigma_{N_{\text{eff}}}. \quad (2.6)$$

In practice, the derivatives, $\partial D / \partial \Delta N_{\text{eff}}$, can be obtained numerically from publicly available codes. In this work, we use Parthenope [22].

Immediately following BBN, the primordial abundances in the patches are conserved. As the Universe expands, and overdensities collapse to form galaxies, variations on scales smaller than those scales that collapse to form galaxies get mixed. Measurements from different galaxies are therefore sensitive to isocurvature fluctuations down to galactic scales. Consequently, the scale λ entering in eq. (2.3) is the comoving size of a patch, λ_{gal} , which collapses to form the galaxies we observe

$$\lambda_{\text{gal}} = 3.7 \left(\frac{M_{\text{gal}}}{10^{12} M_{\odot}} \right)^{1/3} \left(\frac{\Omega_{\text{m}} h^2}{0.14} \right)^{-1/3} \text{ Mpc}, \quad (2.7)$$

where M_{gal} is the mass of the galaxy. The scale λ_{gal} is larger than the horizon during BBN, $\sim \text{kpc}$, which implies that our analysis built on eq. (2.4) is self-consistent.

The value of ΔN_{eff} experienced by a galaxy is sampled from a distribution with mean $\Delta \bar{N}_{\text{eff}}$ and variance $\sigma_{N_{\text{eff}}}$. Moreover, $\sigma_{N_{\text{eff}}}$ is related to the power spectrum of isocurvature fluctuation, P_S , as

$$\sigma_{N_{\text{eff}}}^2 = \frac{16}{9} \Delta \bar{N}_{\text{eff}}^2 \langle \Delta S_{DR}^2 \rangle = \frac{16}{9} \frac{\Delta \bar{N}_{\text{eff}}^2}{\left[\int d^3x W_{\lambda_{\text{gal}}/2}(\vec{x}) \right]^2} \int_0^{\infty} \frac{dk}{k} |W_{\lambda_{\text{gal}}/2}(k)|^2 \frac{k^3 P_S(k)}{2\pi^2}. \quad (2.8)$$

Since the details of galaxies providing He/H or D/H are usually not observable, the accurate estimation of $W_{\lambda_{\text{gal}}/2}$ is not feasible. Consequently, we cannot exactly relate the variance in the average isocurvature experienced by a galaxy, $\langle \Delta S_{DR}^2 \rangle$, to the isocurvature power spectrum. However, we can obtain an approximate relation between $\langle \Delta S_{DR}^2 \rangle$ and P_S . Assuming a blue-tilted isocurvature power spectrum

$$\Delta_S^2 \equiv \frac{k^3 P_S(k)}{(2\pi^2)} \propto k^n, \quad (2.9)$$

with $n > 0$, and assuming a spherical Gaussian window function, $W_{\lambda/2}(k) = \exp(-k^2 \lambda^2/8)$, eq. (2.8) yields

$$\langle \Delta S_{DR}^2 \rangle = \frac{\Gamma(n/2)}{2} \Delta_S^2 (2\lambda_{\text{gal}}^{-1}). \quad (2.10)$$

Here $\Gamma(x)$ is the Euler Gamma function. As $\langle \Delta S_{DR}^2 \rangle$ determines $\sigma_{N_{\text{eff}}}$ which in turn informs the variance in D/H (or He/H) ratios, the intrinsic variance in the D/H (or He/H) ratio in a given galaxy is determined by dark-radiation isocurvature at scales $\sim \lambda_{\text{gal}}/2$.

3 Constraints from He/H and D/H data

In this section we use data from observations of the ratios of He/H and D/H to place constraints on dark-radiation isocurvature. We first describe the datasets which we use for our analysis and then describe our methodology for D/H and He/H data separately.

3.1 Datasets

D/H measurements are taken from gas clouds that are seen in absorption against the light of an unrelated background quasar [23]. Correspondingly, by looking at the frequency distribution of the light from the quasar, one can estimate the redshift of the gas cloud as well as the column densities of neutral Hydrogen and Deuterium atoms.

For our analysis we use the D/H measurements provided in Ref. [17]. The data uses measurements from seven damped Lyman- α systems¹ around redshifts $z \sim 2 - 3$, that satisfy the strict selection criteria of precision stated in Ref. [25]. To estimate the comoving scale in the early universe from which the gas cloud formed, we require the mass of the gas cloud. While the masses of individual damped Lyman- α systems are not known, their masses have been estimated to be in the range $10^{11} - 10^{12} M_{\odot}$ [26, 27].

The He abundance is derived from observations of the helium and hydrogen emission lines from H II regions in low-metallicity blue compact dwarf galaxies that have undergone little chemical evolution [28]. Regions with minimal chemical evolution are selected so as to minimize He enrichment by stellar processes. However, there still remains some contamination that leads to an increase in the He/H ratio over its primordial value.

In this study we use He/H data provided in Ref. [18]. The data consists of 15 measurements of He II regions from 14 different galaxies. For our analysis, we assume that each galaxy has a uniform value of the primordial He/H ratio. Correspondingly, we combine the two measurements of the same galaxy into a single data point using a weighted average. Unlike in the case of Deuterium measurements, the galaxies providing Helium measurements have low redshifts $z < 0.05$. Out of the 14 galaxies used in measuring He/H abundance we find the masses of three² of them in the SPARC database [29]. Their masses are in the range $10^{10.2} - 10^{10.6} M_{\odot}$.

3.2 Constraints from D/H data

The gas in damped Lyman- α systems is assumed not to have produced or destroyed significant amounts of Deuterium. Correspondingly, the measurement from a gas cloud samples the primordial value of D which is assumed to be drawn from a distribution with mean and variance given by $\{\bar{D}, \sigma_d\}$. The probability of getting a measurement of D_i from gas cloud i is then given by

$$P(D_i|\{\bar{D}, \sigma_d\}) = \frac{1}{\sqrt{2\pi(\sigma_{n,i}^2 + \sigma_d^2)}} \exp\left(-\frac{(D_i - \bar{D})^2}{2(\sigma_{n,i}^2 + \sigma_d^2)}\right), \quad (3.1)$$

where $\sigma_{n,i}$ is the estimated noise in the measurement of D . We have assumed that each measurement has the same intrinsic variance in D . We do so because the damped Lyman- α systems typically have masses in the relatively narrow range $10^{11} - 10^{12} M_{\odot}$ [26, 27]. Correspondingly, the gas clouds in our data have roughly the same λ_{gal} (see eq. (2.7)) and thus the same variance in D (see eqs. (2.10) and (2.6)). Moreover, we have neglected covariance between different measurements. This approximation is valid because isocurvature on the scales of separation between different galaxies in our data (usually > 100 Mpc) is constrained by CMB measurements [11] to be much smaller than the variance to which our analysis is sensitive.

¹The damped Lyman- α systems are distinct from the Lyman- α forest systems which provide matter structure constraints around $\gtrsim 1$ Mpc. They are differentiated on the basis of the amount of neutral Hydrogen column densities, $N(\text{H I})$. Lyman- α forest systems are those with $N(\text{H I}) < 10^{17} \text{cm}^{-2}$ and damped Lyman- α systems are those with $2 \times 10^{20} \text{cm}^{-2} < N(\text{H I})$ [24].

²The galaxies of whose masses we found are aliased as Mrk 209, Mrk 71 and SBS 1415+437 in [18]. While their aliases used in SPARC database are UGCA 281, NGA 2366, and PGC51017, respectively.

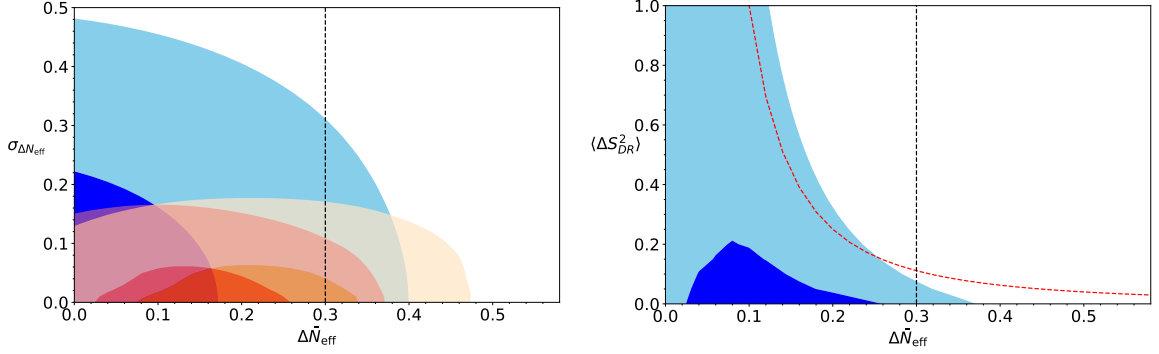


Figure 1: *Left:* 1σ and 2σ constraints on $\{\Delta\bar{N}_{\text{eff}}, \sigma_{\Delta N_{\text{eff}}}\}$ from He/H data (blue contours), D/H data (orange contours) and from combined data (red contours). The vertical dashed line denotes the upper limit on ΔN_{eff} from Planck data with 95% confidence [19]. *Right:* Constraints on $\{\Delta\bar{N}_{\text{eff}}, \langle\Delta S_{\text{DR}}^2\rangle\}$ from combined data. Here ΔS_{DR} is the average dark radiation in a galaxy. For blue-tilted isocurvature mode $\langle\Delta S_{\text{DR}}^2\rangle$ is approximately same as the normalized isocurvature power spectrum at 1 Mpc, $\Delta_S^2(1\text{Mpc}^{-1})$ (see eq. (2.10)). The red-dashed line marks the parameters space at which $\Delta\bar{N}_{\text{eff}}\Delta S_{\text{DR}} = 0.1$. Correspondingly, the small $\Delta\bar{N}_{\text{eff}}\Delta S_{\text{DR}}$ approximation made in eq. (2.4) holds for most of our parameter space.

The constraints from D_i measurements are degenerate in ΔN_{eff} and $\Omega_b h^2$. To remove this degeneracy we fix the value of $\Omega_b h^2$ using the Planck data,³ $\Omega_b h^2 = 0.02239 \pm 0.00018 \equiv \bar{\Omega}_b h^2 \pm \sigma_{\Omega_b}$ [19], where σ_{Ω_b} is the uncertainty on the baryon density, which is assumed to be spatially homogeneous. The corresponding likelihood function is then given by

$$\mathcal{L}_0(\Delta N_{\text{eff}}, \sigma_{\Delta N_{\text{eff}}}) = \int_0^\infty \left[\prod_i P(D_i | \{\bar{D}, \sigma_d\}) \right]_{\Delta N_{\text{eff}}, \Omega_b h^2, \sigma_{N_{\text{eff}}}} \frac{\exp\left(-\frac{(\Omega_b h^2 - \bar{\Omega}_b h^2)^2}{2\sigma_{\Omega_b}^2}\right)}{\sqrt{2\pi\sigma_{\Omega_b}^2}} d(\Omega_b h^2). \quad (3.2)$$

We numerically marginalize over $\Omega_b h^2$ to obtain our likelihood estimate.

Using Parthenope [22] to estimate $D(\Delta N_{\text{eff}}, \Omega_b h^2)$ and $\frac{\partial D}{\partial \Delta N_{\text{eff}}}$, we find the 1σ and 2σ limits on $\{\Delta\bar{N}_{\text{eff}}, \sigma_{N_{\text{eff}}}\}$ shown as orange contours in left panel of figure 1.

3.3 Constraints from He/H data

The methodology used in analysing D/H data is also applicable for He/H data after accounting for the He produced by stellar processes. To estimate the amount of primordial He/H ratio, Y_p , in a given galaxy we assume a linear relation between the Oxygen to Hydrogen ratio (O/H) and the He/H ratio produced by stellar processes. Thus the net He/H ratio, Y , found in a galaxy is given by

$$Y = Y_p + m \times (\text{O/H}), \quad (3.3)$$

where m is the proportionality between O/H production and He/H production through stellar processes. Above, Y_p fluctuates with ΔN_{eff} in a similar manner as in eq. (2.5), except with

³The Planck constraints on $\Omega_b h^2$ are slightly degenerate with N_{eff} . Correspondingly we take Planck constraints on $\Omega_b h^2$ values marginalised over N_{eff} from TT+TE+EE+lowl+lowlE+BAO data.

D replaced by Y_p . Similarly, the variance in Y_p , given by σ_y , and the variance in ΔN_{eff} fluctuations are related by eq. (2.6), except with D replaced by Y_p .

Taking into account the linear relation between O/H and Y , the probability of getting a measurement of Y_i from galaxy i is given by

$$\tilde{P}(Y_i|\{\bar{Y}_p, \sigma_y, m\}) = \frac{1}{\sqrt{2\pi(\sigma_{n,i}^2 + \sigma_y^2 + m^2\sigma_{\text{On},i}^2)}} \exp\left(-\frac{(Y_i - (\bar{Y}_p + m(\text{O/H})_i))^2}{2(\sigma_{n,i}^2 + \sigma_y^2 + m^2\sigma_{\text{On},i}^2)}\right), \quad (3.4)$$

where $\sigma_{\text{On},i}$ is the noise in O/H measurement. Just like in the case of Deuterium, we have considered all galaxies to have the same variance in ΔN_{eff} and neglected covariance between different galaxies. The corresponding likelihood function is then given by

$$\begin{aligned} \mathcal{L}(\Delta N_{\text{eff}}, \sigma_{N_{\text{eff}}}) &= \int_0^\infty \int_0^\infty \left[\prod_i \tilde{P}(Y_i|\{\bar{Y}, \sigma_y, m\}) \right]_{\Delta N_{\text{eff}}, \Omega_b h^2, \sigma_{N_{\text{eff}}}} \\ &\quad \times \frac{\exp\left(-\frac{(\Omega_b h^2 - \bar{\Omega}_b h^2)^2}{2\sigma_{\Omega_b}^2}\right)}{\sqrt{2\pi\sigma_{\Omega_b}^2}} dm d(\Omega_b h^2). \end{aligned} \quad (3.5)$$

Since $m \ll 1$, we can neglect $m^2\sigma_{\text{On},i}^2$ above. Moreover, using the definition of \mathcal{L}_0 in eq. (3.2) but with D replaced by Y , the above integral simplifies to,

$$\begin{aligned} \mathcal{L}(\Delta N_{\text{eff}}, \sigma_{N_{\text{eff}}}) &\approx \mathcal{L}_0(\Delta N_{\text{eff}}, \sigma_{N_{\text{eff}}}) \\ &\quad \times \int_0^\infty \exp\left(-\frac{1}{2} \left[\sum_i \frac{(\text{O/H})_i^2}{(\sigma_{n,i}^2 + \sigma_y^2)} \right] m^2 + \left[\sum_i \frac{(Y_i - \bar{Y})(\text{O/H})_i}{(\sigma_{n,i}^2 + \sigma_y^2)} \right] m\right) dm \\ &= \mathcal{L}_0(\Delta N_{\text{eff}}, \sigma_{N_{\text{eff}}}) \frac{\sqrt{\pi} e^{b^2/(2a)} \left(\text{erf}\left(\frac{b}{\sqrt{2a}}\right) + 1\right)}{\sqrt{a}}, \end{aligned} \quad (3.6)$$

where a and b are the inverse variance weighted sum of $(\text{O/H})_i^2$ and $(Y_i - \bar{Y})(\text{O/H})_i$ respectively (terms in the square bracket in the first line). Using Parthenope [22] to estimate $Y(\Delta N_{\text{eff}}, \Omega_b h^2)$ and $\frac{\partial Y}{\partial \Delta N_{\text{eff}}}$ we find the 1σ and 2σ limits on $\{\Delta \bar{N}_{\text{eff}}, \sigma_{N_{\text{eff}}}\}$, shown as blue contours in left panel of figure 1.

The red contours in the left panel of figure 1 show the combined constraints from Helium and Deuterium data, which restricts the variance in ΔN_{eff} to be $\sigma_{N_{\text{eff}}} \leq 0.17$ at 95% confidence. In the right panel of figure 1 we convert the constraints on $\sigma_{N_{\text{eff}}}$ to constraints on $\langle \Delta S_{\text{DR}}^2 \rangle$ using eq. (2.8). Since the masses of the galaxies used in our measurements lie in the range $10^{10} - 10^{12} M_\odot$, we consider all our measurements to have $\lambda_{\text{gal}} \sim 2$ Mpc (see eq. (2.7)). Correspondingly, the variance in average dark radiation isocurvature in a galaxy, $\langle \Delta S_{\text{DR}}^2 \rangle$ approximately measures isocurvature on scales around $\lambda_{\text{gal}}/2 \sim 1$ Mpc, i.e. $\langle \Delta S_{\text{DR}}^2 \rangle \sim \Delta_S^2(k \sim 1 \text{Mpc}^{-1})$ (see eq. (2.10)). The constraints on isocurvature become significantly weaker for smaller values of $\Delta \bar{N}_{\text{eff}}$. This is indicative of the fact that smaller dark radiation densities make it harder for the isocurvature component to gravitationally affect BBN.

4 Discussion and conclusions

In a universe with a dark radiation field that is populated independently of the SM sector following inflation, an isocurvature mode can naturally occur between the two sectors. In this

work, we have demonstrated that such an isocurvature mode leads to spatially varying BBN yields. Correspondingly, we have derived constraints on the existence of an isocurvature mode between SM plasma and putative dark radiation by looking at spatial variations in He/H and D/H abundances.

A lack of excess variance in observed He/H and D/H data limits the amount of isocurvature present during BBN. Assuming each galaxy has internally uniform He/H and D/H ratios, a single galaxy probes dark radiation isocurvature at scales $\sim \lambda_{\text{gal}}/2$. Here λ_{gal} corresponds to the comoving size of the overdensity which eventually collapses to form the galaxy in question. Since the structures which provide He/H or D/H measurements typically have masses around $10^{11} M_{\odot}$, our analysis is sensitive to dark radiation isocurvature at scales ~ 1 Mpc. Subsequently, using He/H data from measurements of nearby galaxies [17] and D/H data from measurements of high-redshift Lyman- α absorption systems [18], we constrained the variance of average dark radiation isocurvature fluctuations, to be $\sqrt{\langle \Delta S_{\text{DR}}^2 \rangle} < 0.13/\Delta \bar{N}_{\text{eff}}$ (see right panel of figure 1) at 95% confidence. The quantity $\langle \Delta S_{\text{DR}}^2 \rangle$ is approximately the same as the normalized isocurvature power spectrum at 1 Mpc. The exact relation between $\langle \Delta S_{\text{DR}}^2 \rangle$ and the isocurvature power spectrum requires an accurate estimation of the primordial overdensities that collapse to form the galaxies in our data. Finally, we also constrain the variance in ΔN_{eff} to be $\sigma_{N_{\text{eff}}} < 0.17$ at 95% confidence.

By translating the neutrino isocurvature constraints by Planck [11] to dark radiation isocurvature,⁴ we find that dark radiation isocurvature fluctuations are constrained to be less than $\sim 10^{-5} \times N_{\text{eff}}/\Delta \bar{N}_{\text{eff}}$ on scales larger than ~ 10 Mpc. Although the CMB is much more sensitive probe than the He/H and D/H data, the latter is able to probe isocurvature at scales that are inaccessible to CMB measurements.

If dark radiation and dark matter fluctuations are correlated—which could occur, for example, in theories of dark freeze-out in the presence of isocurvature—then constraints from measurements of clustering in the Lyman- α forest on dark matter isocurvature can be translated to dark radiation. The Lyman- α forest data constraints DM isocurvature to be less than 10^{-4} at 1 Mpc [30], by putting limits on the excess power over the adiabatic matter power spectrum extrapolated from CMB measurements. In contrast, the analysis in this study is sensitive directly to the isocurvature mode between dark radiation and the SM sector, and is unaffected by the adiabatic fluctuations.

The extension of constraints from Lyman- α forest data to smaller scales is limited by solving non-linear structure formation—a complication that does not affect our analysis. In contrast, the techniques used in this study can theoretically be used to extend the constraints down to scales ~ 0.01 Mpc, i.e. scales slightly larger than the comoving horizon during BBN. To achieve the constraints at such small scales one would require measurements of He/H or D/H from structures with masses of order $\sim 10^6 - 10^7 M_{\odot}$. Potential future measurements of He/H in halos of masses $\sim 10^{9.5} M_{\odot}$ [31] would extend the constraints down to ~ 0.3 Mpc.

Acknowledgments

We thank Brian Fields for useful discussions. We thank Ofelia Pisanti and Ken Nollett for providing help in implementing Parthenope. The work of PA and PR is supported in

⁴CMB measurements cannot distinguish between the effects from dark-radiation and neutrinos. Consequently the isocurvature, \mathcal{S} constrained by CMB would have contributions from both dark-radiation and neutrinos, $\mathcal{S} = \frac{3}{4} \left(\frac{\delta \rho_{\text{DR}} + \delta \rho_{\nu}}{\rho_{\text{DR}} + \rho_{\nu}} - \frac{\delta \rho_{\gamma}}{\rho_{\gamma}} \right) = \frac{\rho_{\text{DR}}}{\rho_{\text{DR}} + \rho_{\nu}} \mathcal{S}_{\text{DR}} + \frac{\rho_{\nu}}{\rho_{\text{DR}} + \rho_{\nu}} \mathcal{S}_{\nu}$. The subscript ν refer to quantities for neutrinos.

part by NASA Astrophysics Theory Grant NNX17AG48G. PA thanks the Kavli Institute for Theoretical Physics for hospitality and support through National Science Foundation Grant No. NSF PHY-1748958 as this work was nearing completion. This work was supported by Brand and Monica Fortner.

A Dark radiation isocurvature as spatially varying N_{eff}

In this appendix, we demonstrate that, on super-horizon scales, the effect of an isocurvature mode between dark radiation and the visible sector is to vary the local value of the effective number of degrees of freedom, N_{eff} . We begin by reviewing the separate Universe principle, before showing explicitly how a dark-radiation isocurvature mode may be interpreted as a spatially varying effective number of relativistic species, $N_{\text{eff}}(\vec{x})$.

A.1 Separate universe principle and total density fluctuations

The separate universe principle (see, e.g., Refs. [20, 21]) posits that each super-horizon sized patch can be treated as an isolated, independent, Friedman-Robertson-Walker (FRW) universe. Any fluctuations on scales larger than the horizon simply become a part of the background variables of that island universe.

We begin by demonstrating that zero-mode fluctuations (Fourier mode $k = 0$) can be absorbed into the background quantities (density, pressure, etc.). The reason is straightforward. After fixing our coordinate system (fixing the gauge), there remains a residual coordinate transformation which can be used to absorb the fluctuations into a redefinition of the background. This can be seen explicitly as follows. We write the perturbed FRW metric as

$$[g_{\mu\nu}] = \begin{bmatrix} -(1+2\psi) & -a\partial_i\beta \\ -a\partial_i\beta & a^2[(1+2\phi)\delta_{ij} + 2\partial_i\partial_j\gamma] \end{bmatrix}. \quad (\text{A.1})$$

Under an infinitesimal coordinate transformation (gauge transformation) $x^{\mu'} = x^\mu + \xi^\mu$, with $\xi_i = \partial_i\xi$, the scalar parts of the metric perturbations transform as

$$\begin{aligned} \psi' &= \psi - \dot{\xi}^0, & \beta' &= \beta - \frac{1}{a}\xi^0 + a\dot{\xi}, \\ \phi' &= \phi - H\xi^0, & \gamma' &= \gamma - \xi. \end{aligned} \quad (\text{A.2})$$

The two scalar parts of the coordinate transformation, ξ^0 and ξ , can be used to set two of the four scalar perturbations in eq. (A.1) to zero. In conformal Newton gauge, ξ^0 and ξ are chosen to set $\beta = \gamma = 0$ and make the metric diagonal. However, because only gradients of β and γ appear in the metric, spatially uniform changes of coordinates leave the metric diagonal. Specifically, consider a transformation of the conformal Newton metric given by

$$\xi^0 = \epsilon(t) \quad \xi = \omega x^i x^j \delta_{ij}, \quad (\text{A.3})$$

where ω is a constant. The metric perturbations transform as

$$\psi' = \psi - \dot{\epsilon} \quad \beta' = -\frac{1}{a}\epsilon(t), \quad (\text{A.4})$$

$$\phi' = \phi - H\epsilon(t) \quad \gamma' = -\omega x^i x^j \delta_{ij}. \quad (\text{A.5})$$

Because only spatial derivatives of β and γ appear in the metric, the transformation in eq. (A.3) leaves the metric diagonal. The diagonal term from γ' can be absorbed into ϕ to give

$$\psi' = \psi - \dot{\epsilon}, \quad (\text{A.6})$$

$$\phi' = \phi - H\epsilon(t) + \partial_i \partial_i \gamma' / 3 = \phi - H\epsilon(t) - 2\omega. \quad (\text{A.7})$$

The transformation as described in eq. (A.3) keeps the metric diagonal and is a residual gauge freedom for conformal Newton gauge. This residual gauge freedom in eqs. (A.6) and (A.7) can be used to remove the spatially homogeneous fluctuations in ϕ and ψ , and set the $k = 0$ Fourier mode to zero, $\phi'_{k=0} = \psi'_{k=0} = 0$, giving the relations

$$H\epsilon + 2\omega = \phi_{k=0}, \quad \dot{\epsilon} = \psi_{k=0}. \quad (\text{A.8})$$

In the absence of metric perturbations, the Einstein equations imply that the total density perturbation vanishes. We can demonstrate this explicitly by noting that, under the residual gauge transformation, eq. (A.3), the density perturbation transforms as

$$\delta\rho' = \delta\rho - \dot{\rho}\epsilon = \frac{1}{4\pi G}(4\pi G\delta\rho - 3H\dot{H}\epsilon), \quad (\text{A.9})$$

where in the second equality we used Friedmann equation for the background, $H^2 = 8\pi G\rho/3$. Further, because $\omega = \text{const.}$, eq. (A.8) gives us the relation

$$\dot{H}\epsilon = \dot{\phi}_{k=0} - H\psi_{k=0}. \quad (\text{A.10})$$

Substituting this result into the gauge transformation given in eq. (A.9) for $k = 0$ mode, we obtain

$$\delta\rho'_{k=0} = \frac{1}{4\pi G}(4\pi G\delta\rho_{k=0} - 3H\dot{\phi}_{k=0} + 3H^2\psi_{k=0}). \quad (\text{A.11})$$

The above vanishes identically after using the Einstein equation for $\delta\rho_{k=0}$. The residual gauge transformation in eq. (A.3) self-consistently removes all zero mode perturbations in the total density. The shift ϵ that is required to gauge away the perturbations is simply a uniform shift in coordinate time.

While the above analysis holds exactly for $k = 0$ mode, it can be extended to superhorizon modes up to corrections of order $O(k^2/(aH)^2)$. To see this, consider a Universe with a single superhorizon mode fluctuation, ϕ_k with $k \ll aH$. On a patch of the Universe with a scale sufficiently small compared to k^{-1} , but still large compared to the horizon, the fluctuation ϕ_k appears almost constant. If we consider two such patches separated by a distance comparable to k^{-1} , each patch samples a different approximately uniform value of ϕ_k . Consequently, in each patch, we may use the residual gauge freedom to remove this approximately constant ϕ_k . The approximately uniform shift in coordinate needed to make each patch uniform is different in each patch. Due to the equivalence principle, the only observable effects of such a shift enter at order $O(k^2/(aH)^2)$.

A.2 Adiabatic vs isocurvature perturbations and residual gauge shifts

Above we showed that the total density fluctuations can be removed on super-horizon scales. However, if the Universe is filled with a multi-component fluid, the perturbations in each fluid species need not necessarily vanish after this procedure. In fact, only adiabatic perturbations

in each species necessarily vanish, as we now demonstrate. Adiabatic perturbations between different species are related by

$$\frac{\delta\rho_1}{\dot{\rho}_1} = \frac{\delta\rho_2}{\dot{\rho}_2} = \frac{\delta\rho_3}{\dot{\rho}_3} = \dots = \epsilon \quad (\text{A.12})$$

where ϵ is the quantity obtained by solving eq. (A.8). We also show that isocurvature perturbations do not in general vanish, but can be absorbed into the background quantities within each patch. In a Universe with isocurvature perturbations, separate Universes evolve with both shifted clocks due to the background adiabatic fluctuations, but also spatially varying background densities, as we now demonstrate.

Consider now a universe comprised of two non-interacting perfect fluids, with densities ρ_1 and ρ_2 . We suppose that on large scales $k^{-1} \gg (aH)^{-1}$, there exist density fluctuations in both species. We then consider a patch of the Universe small compared to k^{-1} but large compared to the horizon. In this patch, after the residual gauge shift with magnitude specified by eq. (A.8), the total density perturbation in this patch vanishes giving

$$\delta\rho'_{tot} = \delta\rho'_1 + \delta\rho'_2 = 0. \quad (\text{A.13})$$

However, note that this only constrains the total density to vanish; it is not necessary for individual $\delta\rho'_i$ to also vanish. When they do, then using eq. (A.9), we see that the species satisfy eq. (A.12).

For an isocurvature mode, the density perturbations in individual species do not vanish after the gauge shift

$$\delta\rho'_1 = -\delta\rho'_2 \neq 0. \quad (\text{A.14})$$

However, these isocurvature perturbations can be absorbed into the background variables. To see this explicitly we consider the zero-mode density-perturbation equation,

$$\delta\dot{\rho}_i + 3H(1 + w_i)\delta\rho_i + 3\rho_i\dot{\phi} = 0, \quad (\text{A.15})$$

where $i = 1, 2$ and w_i is the equation of state of the i -th perfect fluid. After gauge shift this becomes

$$\delta\dot{\rho}'_i + 3H(1 + w_i)\delta\rho'_i = 0, \quad (\text{A.16})$$

which can be trivially absorbed into a redefinition of the background density

$$\tilde{\rho}_i = \rho_i + \delta\rho'_i. \quad (\text{A.17})$$

This redefinition will not affect the metric or other Einstein variables as they only depend on total density in the universe, which remains unchanged after the absorption of isocurvature perturbations.

A.3 Dark-radiation isocurvature and the spatial variation of N_{eff}

In the main body of the paper we are primarily concerned with patches of size $\lambda_{\text{gal}} \sim 1$ Mpc, the matter inside of which collapses to form the galaxies from which we obtain He/H and D/H measurements. Since the horizon size during BBN, ~ 1 Kpc, is much smaller than λ_{gal} , we can use the separate universe principle to calculate the variation in ΔN_{eff} due to isocurvature between the dark radiation and the SM radiation bath in different galaxy-sized patches.

Consider a spherical volume of radius $r = \lambda_{\text{gal}}/2$, the matter within which later collapses to form a galaxy. Let ρ_1 and ρ_2 be the homogeneous densities of the SM and dark radiation respectively. In the previous sub-section we showed that an isocurvature fluctuation, $\delta\rho'_i(k)$, of a superhorizon-sized mode can be absorbed into the homogeneous density. For the spherical patch we are considering, using the separate universe principle, we can absorb the net $\delta\rho'_i(\vec{x})$ inside the volume into the homogeneous density (using eq. (A.17) and eq. (A.14)),

$$\tilde{\rho}_1 = \rho_1 + \Delta\rho'_2 \qquad \tilde{\rho}_2 = \rho_2 - \Delta\rho'_2, \qquad (\text{A.18})$$

where $\Delta\rho'_2 = -\Delta\rho'_1$ is the average isocurvature fluctuation in the dark radiation inside a spherical volume of radius r ,

$$\Delta\rho'_2 = \int_0^\infty \frac{d^3x}{V_r} \delta\rho'_2(\vec{x}) W_r(\vec{x}). \qquad (\text{A.19})$$

Here W_r is a window function which weights the integral to be within r radius from origin and V_r is the volume swept by the window function, $V_r = \int d^3x W_r(\vec{x})$. The spherical volume effectively has $\tilde{\rho}_i$ as its homogeneous density. Note that while $\Delta\rho'_2$ involves contributions from all Fourier modes, the contribution from modes $k^{-1} \ll r$ is suppressed. The suppression is because the small wavelength modes have around the same number of over-densities and under-densities in a patch much larger than the mode's wavelength. Consequently, the super-horizon assumption in eq. (A.18) approximately holds as long as r is super-horizon sized.

Due to the presence of isocurvature, N_{eff} inside the spherical volume is also modified

$$\Delta N_{\text{eff}} \propto \frac{\tilde{\rho}_2}{\tilde{\rho}_1} = \frac{\rho_2 + \Delta\rho'_2}{\rho_1 - \Delta\rho'_2}. \qquad (\text{A.20})$$

In the main body of paper we define dark radiation isocurvature with respect to photons in eq. (2.2). However, as photons are adiabatic with SM plasma the isocurvature perturbation can equivalently be written as

$$S_{DR} = \frac{3}{4} \left(\frac{\delta\rho_2}{\rho_2} - \frac{\delta\rho_1}{\rho_1} \right) = \frac{3}{4} \frac{\rho_1\rho_2}{\rho_1 + \rho_2} \delta\rho'_2. \qquad (\text{A.21})$$

In the second equality above we have expressed S_{DR} in the uniform density gauge where $\delta\rho'_2 = -\delta\rho'_1$. Consequently, the average isocurvature in the spherical volume is given by

$$\Delta S_{DR} = \int_0^\infty \frac{d^3x}{V_r} S_{DR}(\vec{x}) W_r(\vec{x}) = \frac{3}{4} \frac{\rho_1\rho_2}{\rho_1 + \rho_2} \Delta\rho'_2. \qquad (\text{A.22})$$

Replacing above back in eq. (A.20), we can rewrite ΔN_{eff} as

$$\Delta N_{\text{eff}} \propto \frac{\rho_2}{\rho_1} \frac{1 + \frac{4}{3} \frac{1}{1+\rho_2/\rho_1} \Delta S_{DR}}{1 - \frac{4}{3} \frac{\rho_2/\rho_1}{1+\rho_2/\rho_1} \Delta S_{DR}} \xrightarrow{(\rho_2/\rho_1)\Delta S_{DR} \ll 1} \frac{\rho_2}{\rho_1} \left(1 + \frac{4}{3} \Delta S_{DR} \right). \qquad (\text{A.23})$$

Thus ΔN_{eff} is sensitive to the average isocurvature in the spherical volume within the window function.

Since ΔS_{DR} depends on position, it varies between galaxies. The variance in ΔS_{DR} is given by

$$\langle \Delta S_{DR}^2 \rangle = \frac{1}{V_r^2} \int \frac{dk}{k} |W_r(k)|^2 \Delta_S^2(k), \qquad (\text{A.24})$$

where $\Delta_S^2 = k^3 P_S(k)/(2\pi^2)$, and $W_r(k)$ and $P_S(k)$ are the Fourier transforms of $W_r(\vec{x})$ and $\langle S_{DR}(\vec{x})S_{DR}(\vec{x}') \rangle$ respectively. Since the contribution of small wavelength modes, $kr \gg 1$, is suppressed in r sized patch, $W_r(k)$ is very small for $k \gg r^{-1}$. Consequently for a blue-tilted isocurvature power spectrum ($\Delta_S^2 \sim k^n$, with $n > 0$), we have

$$\langle \Delta S_{DR}^2 \rangle \sim \Delta_S^2(k \sim r^{-1}). \quad (\text{A.25})$$

Thus, isocurvature on scales near λ_{gal} leads to fluctuations in primordial ΔN_{eff} between different galaxies.

References

- [1] **CMB-S4** Collaboration, K. N. Abazajian *et al.*, “CMB-S4 Science Book, First Edition,” [arXiv:1610.02743](#) [[astro-ph.CO](#)].
- [2] G. Mangano, G. Miele, S. Pastor, T. Pinto, O. Pisanti, and P. D. Serpico, “Relic neutrino decoupling including flavour oscillations,” *Nuclear Physics B* **729** no. 1-2, (Nov, 2005) 221–234. <http://dx.doi.org/10.1016/j.nuclphysb.2005.09.041>.
- [3] E. Grohs, G. Fuller, C. Kishimoto, M. Paris, and A. Vlasenko, “Neutrino energy transport in weak decoupling and big bang nucleosynthesis,” *Physical Review D* **93** no. 8, (Apr, 2016) . <http://dx.doi.org/10.1103/PhysRevD.93.083522>.
- [4] P. F. de Salas and S. Pastor, “Relic neutrino decoupling with flavour oscillations revisited,” *JCAP* **1607** (2016) 051, [arXiv:1606.06986](#) [[hep-ph](#)].
- [5] K. Akita and M. Yamaguchi, “A precision calculation of relic neutrino decoupling,” [arXiv:2005.07047](#) [[hep-ph](#)].
- [6] J. Errard, S. M. Feeney, H. V. Peiris, and A. H. Jaffe, “Robust forecasts on fundamental physics from the foreground-obscured, gravitationally-lensed CMB polarization,” *JCAP* **1603** (2016) 052, [arXiv:1509.06770](#) [[astro-ph.CO](#)].
- [7] S. Weinberg, “Must cosmological perturbations remain non-adiabatic after multi-field inflation?,” *Phys. Rev.* **D70** (2004) 083522, [arXiv:astro-ph/0405397](#) [[astro-ph](#)].
- [8] D. H. Lyth, C. Ungarelli, and D. Wands, “The Primordial density perturbation in the curvaton scenario,” *Phys. Rev.* **D67** (2003) 023503, [arXiv:astro-ph/0208055](#) [[astro-ph](#)].
- [9] M. Kawasaki, K. Miyamoto, K. Nakayama, and T. Sekiguchi, “Isocurvature perturbations in extra radiation,” *JCAP* **1202** (2012) 022, [arXiv:1107.4962](#) [[astro-ph.CO](#)].
- [10] E. Kawakami, M. Kawasaki, K. Miyamoto, K. Nakayama, and T. Sekiguchi, “Non-Gaussian isocurvature perturbations in dark radiation,” *JCAP* **1207** (2012) 037, [arXiv:1202.4890](#) [[astro-ph.CO](#)].
- [11] **Planck** Collaboration, Y. Akrami *et al.*, “Planck 2018 results. X. Constraints on inflation,” [arXiv:1807.06211](#) [[astro-ph.CO](#)].
- [12] **Planck** Collaboration, Y. Akrami *et al.*, “Planck 2018 results. I. Overview and the cosmological legacy of Planck,” [arXiv:1807.06205](#) [[astro-ph.CO](#)].
- [13] G. P. Holder, K. M. Nollett, and A. van Engelen, “On Possible Variation in the Cosmological Baryon Fraction,” [arXiv:0907.3919](#) [[astro-ph.CO](#)].
- [14] K. Inomata, M. Kawasaki, A. Kusenko, and L. Yang, “Big Bang Nucleosynthesis Constraint on Baryonic Isocurvature Perturbations,” *JCAP* **1812** no. 12, (2018) 003, [arXiv:1806.00123](#) [[astro-ph.CO](#)].
- [15] C. J. Copi, K. A. Olive, and D. N. Schramm, “Implications of a primordial origin for the dispersion in d/h in quasar absorption systems,” *Submitted to: Astrophys. J.* (1996) , [arXiv:astro-ph/9606156](#) [[astro-ph](#)].

- [16] R. V. Wagoner, “Big-Bang Nucleosynthesis Revisited,” *ApJ* **179** (Jan, 1973) 343–360.
- [17] R. J. Cooke, M. Pettini, and C. C. Steidel, “One Percent Determination of the Primordial Deuterium Abundance,” *Astrophys. J.* **855** no. 2, (2018) 102, [arXiv:1710.11129](#) [[astro-ph.CO](#)].
- [18] E. Aver, K. A. Olive, and E. D. Skillman, “The effects of He I λ 10830 on helium abundance determinations,” *JCAP* **1507** no. 07, (2015) 011, [arXiv:1503.08146](#) [[astro-ph.CO](#)].
- [19] **Planck** Collaboration, N. Aghanim *et al.*, “Planck 2018 results. VI. Cosmological parameters,” [arXiv:1807.06209](#) [[astro-ph.CO](#)].
- [20] S. Weinberg, “Adiabatic modes in cosmology,” *Phys. Rev.* **D67** (2003) 123504, [arXiv:astro-ph/0302326](#) [[astro-ph](#)].
- [21] D. H. Lyth and D. Wands, “The CDM isocurvature perturbation in the curvaton scenario,” *Phys. Rev.* **D68** (2003) 103516, [arXiv:astro-ph/0306500](#) [[astro-ph](#)].
- [22] R. Consiglio, P. F. de Salas, G. Mangano, G. Miele, S. Pastor, and O. Pisanti, “PARthENoPE reloaded,” *Comput. Phys. Commun.* **233** (2018) 237–242, [arXiv:1712.04378](#) [[astro-ph.CO](#)].
- [23] T. F. Adams, “The detectability of deuterium Lyman alpha in QSOs,” *A&A* **50** (Aug., 1976) 461–462.
- [24] A. M. Wolfe, E. Gawiser, and J. X. Prochaska, “Damped $\text{Ly}\alpha$ systems,” *Annual Review of Astronomy and Astrophysics* **43** no. 1, (2005) 861–918. <https://doi.org/10.1146/annurev.astro.42.053102.133950>.
- [25] R. J. Cooke, M. Pettini, R. A. Jorgenson, M. T. Murphy, and C. C. Steidel, “PRECISION MEASURES OF THE PRIMORDIAL ABUNDANCE OF DEUTERIUM,” *The Astrophysical Journal* **781** no. 1, (Jan, 2014) 31. <https://doi.org/10.1088/2F0004-637x/2F781/2F1/2F31>.
- [26] R. Mackenzie, M. Fumagalli, T. Theuns, D. J. Hatton, T. Garel, S. Cantalupo, L. Christensen, J. P. U. Fynbo, N. Kanekar, P. Møller, J. O’Meara, J. X. Prochaska, M. Rafelski, T. Shanks, and J. Trayford, “Linking gas and galaxies at high redshift: MUSE surveys the environments of six damped $\text{Ly}\alpha$ systems at $z \approx 3$,” *MNRAS* (Jun, 2019) 1435, [arXiv:1904.07254](#) [[astro-ph.GA](#)].
- [27] A. Font-Ribera, J. Miralda-Escudé, E. Arnau, B. Carithers, K.-G. Lee, P. Noterdaeme, I. Pâris, P. Petitjean, J. Rich, E. Rollinde, N. P. Ross, D. P. Schneider, M. White, and D. G. York, “The large-scale cross-correlation of Damped Lyman alpha systems with the Lyman alpha forest: first measurements from BOSS,” *JCAP* **2012** no. 11, (Nov, 2012) 059, [arXiv:1209.4596](#) [[astro-ph.CO](#)].
- [28] M. Peimbert and S. Torres-Peimbert, “Chemical composition of H II regions in the Large Magellanic Cloud and its cosmological implications,” *Apj* **193** (Oct., 1974) 327–333.
- [29] P. Li, F. Lelli, S. McGaugh, M. S. Pawlowski, M. A. Zwaan, and J. Schombert, “The halo mass function of late-type galaxies from HI kinematics,” *Astrophys. J.* **886** no. 1, (2019) L11, [arXiv:1911.00517](#) [[astro-ph.GA](#)].
- [30] M. Beltran, J. Garcia-Bellido, J. Lesgourgues, and M. Viel, “Squeezing the window on isocurvature modes with the lyman-alpha forest,” *Phys. Rev.* **D72** (2005) 103515, [arXiv:astro-ph/0509209](#) [[astro-ph](#)].
- [31] C. Sykes, M. Fumagalli, R. Cooke, and T. Theuns, “Determining the primordial helium abundance and UV background using fluorescent emission in star-free dark matter haloes,” [arXiv:1912.06163](#) [[astro-ph.CO](#)].